Four decades of Antarctic Ice Sheet mass balance from 1979–2017

Eric Rignot, Jeremie Mouginot, Bernd Scheuchl, Michiel van den Broeke, Melchior van Wessem, Mathieu Morlighem

Four decades of Antarctic Ice Sheet mass balance from 1979–2017

Eric Rignot[a,b,1], Jérémie Mouginot[a,c], Bernd Scheuchl[a], Michiel van den Broeke[d], Melchior J. van Wessem[d], and Mathieu Morlighem[a]

[a]Department of Earth System Science, University of California, Irvine, CA 92697; [b]Jet Propulsion Laboratory, California Institute of Technology, Pasadena, CA 91109; [c]Institut des Geosciences de l'Environment, Universite Grenoble Alpes, CNRS, 38058 Grenoble, France; and [d]Institute for Marine and Atmospheric Research Utrecht, Utrecht University, 3508 TA Utrecht, The Netherlands

This contribution is part of the special series of Inaugural Articles by members of the National Academy of Sciences elected in 2018.

Contributed by Eric Rignot, December 4, 2018 (sent for review July 30, 2018; reviewed by Richard R. Forster and Leigh A. Stearns)

We use updated drainage inventory, ice thickness, and ice velocity data to calculate the grounding line ice discharge of 176 basins draining the Antarctic Ice Sheet from 1979 to 2017. We compare the results with a surface mass balance model to deduce the ice sheet mass balance. The total mass loss increased from 40 ± 9 Gt/y in 1979–1990 to 50 ± 14 Gt/y in 1989–2000, 166 ± 18 Gt/y in 1999–2009, and 252 ± 26 Gt/y in 2009–2017. In 2009–2017, the mass loss was dominated by the Amundsen/Bellingshausen Sea sectors, in West Antarctica (159 ± 8 Gt/y), Wilkes Land, in East Antarctica (51 ± 13 Gt/y), and West and Northeast Peninsula (42 ± 5 Gt/y). The contribution to sea-level rise from Antarctica averaged 3.6 ± 0.5 mm per decade with a cumulative 14.0 ± 2.0 mm since 1979, including 6.9 ± 0.6 mm from West Antarctica, 4.4 ± 0.9 mm from East Antarctica, and 2.5 ± 0.4 mm from the Peninsula (i.e., East Antarctica is a major participant in the mass loss). During the entire period, the mass loss concentrated in areas closest to warm, salty, subsurface, circumpolar deep water (CDW), that is, consistent with enhanced polar westerlies pushing CDW toward Antarctica to melt its floating ice shelves, destabilize the glaciers, and raise sea level.

glaciology | Antarctica | remote sensing | climate change | sea-level rise

Antarctica contains an ice volume that translates into a sea-level equivalent (SLE) of 57.2 m (1) (Table 1 and *SI Appendix*, Table S1). Its annual net input of mass from snowfall is 2,100 Gt (gigatons = 10^9 tons), excluding ice shelves, equivalent to a 5.8-mm fluctuation in global sea level (2). In a state of mass equilibrium, accumulation of snowfall in the interior should balance surface ablation (wind transport and sublimation) and ice discharge along the periphery into the Southern Ocean. Nearly half of the land ice that crosses the grounding line to reach the ocean to form floating ice shelves melts in contact with the ocean, while the other half breaks up and detaches into icebergs (3, 4).

Recent observations have shown that the ice sheet is losing mass along the periphery due the enhanced flow of its glaciers, at a rate that has been increasing over time, while there is no long-term trend change in snowfall accumulation in the interior [i.e., Antarctica contributes to sea-level rise (SLR) principally via changes in ice dynamics] (5–7). Various techniques have been used to estimate ice sheet mass balance, including (*i*) the component method, which compares accumulation of snowfall over the interior basins with ice discharge by glaciers across the grounding line (where ice becomes afloat in ocean waters and detaches from the bed) at a high resolution (100 m to 1 km); (*ii*) the altimetry method, which measures elevation changes over the entire ice sheet and converts them into mass changes by assuming a density of change at intermediate resolution (1 to 10 km); and (*iii*) the gravity method, which measures directly the relative change in mass on a monthly basis, within centimeters per year, albeit at low resolution (333 km). The techniques have been compared (8–10) to yield reconciled numbers for ice-sheet-wide assessments for the time periods 1992–2011 and 1992–2017, except for East Antarctica, where uncertainties remain.

Here, we present results from the component method updated to 2017 and extending back to 1979, or four decades of observations. We use improved annual time series of ice sheet velocity, updated ice thickness, modeled reconstructions of surface mass balance (SMB), revised drainage inventories, and high-resolution topography to assess the continental ice discharge of 18 regions that include a total of 176 basins, plus the surrounding islands (Fig. 1 and *SI Appendix*, Fig. S1). The period of study covers the entire period of reconstruction of SMB by regional atmospheric climate models. We derive the ice sheet mass balance for 1979–2017, the acceleration in ice mass loss on a decadal time scale (Fig. 2), the partitioning between SMB processes and ice dynamics, the contribution of various regions to the total mass budget, and the implications of the results for the future contribution of Antarctica to SLR.

Results

Antarctica. The total mass loss from Antarctica increased from 40 ± 9 Gt/y in the 11-y time period 1979–1990 to 50 ± 14 Gt/y in 1989–2000, 166 ± 18 Gt/y in 1999–2009, and 252 ± 26 Gt/y in 2009–2017, that is, by a factor 6 (Fig. 2, Table 1, and *SI Appendix*, Fig. S1). This change in mass loss reflects an acceleration of 94 Gt/y per decade in 1979–2017, increasing from

Significance

We evaluate the state of the mass balance of the Antarctic Ice Sheet over the last four decades using a comprehensive, precise satellite record and output products from a regional atmospheric climate model to document its impact on sea-level rise. The mass loss is dominated by enhanced glacier flow in areas closest to warm, salty, subsurface circumpolar deep water, including East Antarctica, which has been a major contributor over the entire period. The same sectors are likely to dominate sea-level rise from Antarctica in decades to come as enhanced polar westerlies push more circumpolar deep water toward the glaciers.

Author contributions: E.R. designed research; J.M. and B.S. performed research; E.R., M.v.d.B., M.J.v.W., and M.M. analyzed data; and E.R. wrote the paper.

Reviewers: R.R.F., University of Utah; and L.A.S., University of Kansas.

The authors declare no conflict of interest.

Data deposition: RACMO data have been deposited on the PANGAEA database, https://www.pangaea.de/ (RACMO2.3p1_ANT27_SMB_yearly_1979_2014; https://doi.pangaea.de/10.1594/PANGAEA.896940).

[1]To whom correspondence should be addressed. Email: erignot@uci.edu.

This article contains supporting information online at www.pnas.org/lookup/suppl/doi:10.1073/pnas.1812883116/-/DCSupplemental.

Published online January 14, 2019.

Table 1. Mass balance of Antarctic glaciers per region (A–K) for the Antarctic Peninsula, West Antarctica, East Antarctica, and total including surrounding islands

Glacier	Region	Area, Mkm^2	SMB_{79-08}, Gt/y	D_{79-89}, Gt/y	D_{89-00}, Gt/y	D_{99-10}, Gt/y	D_{09-17}, Gt/y	M, Gt	SLR, mm	SLE, cm
Larsen D-G	I″-J	61.7	24.8 ± 3.0	24.8[0]	24.8	24.8	24.8 ± 3.0	0	0.0	5
West Graham	I-I″	25.1	89.6 ± 10.4	90.3[4]	91.7	93.7	98.2 ± 5.0	−140	0.4	1
East Graham	I-I″	4.4	3.3 ± 1.0	3.3[0]	3.3	3.3	3.3 ± 1.0	0	0.0	0
Larsen C	I-I″	18.1	14.5 ± 2.1	15.1[3]	15.9	15.2	15.3 ± 2.0	−32	0.1	1
Larsen B	I-I″	9.0	6.4 ± 0.9	7.3 [4]	7.4	12.5	16.2 ± 1.4	−160	0.4	0
Drygalski	I-I″	1.0	1.4 ± 0.2	1.4[4]	2.4	5.4	5.5 ± 0.6	−83	0.2	0
Larsen A	I-I″	1.3	1.3 ± 0.1	1.3 [4]	2.2	5.0	3.3 ± 0.1	−60	0.2	0
Wordie	I-I″	10.6	14.8 ± 1.9	16.0[1]	17.7	18.8	21.5 ± 1.4	−138	0.4	1
Wilkins	I-I″	14.7	14.6 ± 0.8	14.6[0]	14.6	14.6	14.6 ± 0.8	0	0.0	1
George VI	H′-I	80.1	70.3 ± 4.0	72.6[1]	74.4	78.5	79.1 ± 4.7	−217	0.6	15
Stange	H′-I	15.0	16.5 ± 1.0	19.8[2]	17.6	19.2	18.9 ± 1.3	−91	0.3	2
Antarctic Peninsula		280	293 ± 27	302	307	326	336 ± 26	−909	2.5	28
Ronne	J-J″	644.7	149.4 ± 8.5	152.3[5]	152.1	151.0	149.8 ± 8.0	−77	0.2	158
Fox	H-H′	4.0	5.1 ± 0.3	5.4[2]	7.0	8.2	9.3 ± 0.6	−85	0.2	1
Ferrigno	H-H′	9.4	7.3 ± 0.4	11.3[2]	13.6	13.9	13.3 ± 1.0	−218	0.6	2
Venable	H-H′	14.9	12.7 ± 0.8	14.7[2]	17.8	17.5	16.7 ± 0.9	−152	0.4	3
Abbot	H-H′	26.7	29.2 ± 1.6	30.0[2]	30.9	35.0	30.4 ± 2.5	−96	0.3	4
Cosgrove	G-H	8.0	5.4 ± 0.3	5.3[1]	5.1	5.3	5.2 ± 0.6	6	0.0	1
Pine Island	G-H	181.4	72.5 ± 4.6	80.2[1]	89.5	106.5	133.2 ± 5.8	−1066	3.0	51
Thwaites	G-H	192.8	82.4 ± 4.9	87.0[1]	94.2	101.5	117.3 ± 3.9	−634	1.8	65
Haynes	G-H	9.8	8.0 ± 0.5	10.9[1]	11.2	11.9	12.9 ± 1.0	−139	0.4	2
Crosson	G-H	12.8	9.7 ± 0.5	13.9[1]	18.5	23.4	30.5 ± 1.4	−435	1.2	3
Dotson	G-H	17.4	16.3 ± 0.9	17.1[1]	19.0	22.8	30.0 ± 2.0	−211	0.6	3
Getz	F-G	85.9	73.2 ± 4.4	76.6[5]	76.2	90.3	90.0 ± 4.8	−363	1.0	22
Land	F-G	13.3	10.6 ± 0.6	12.9[5]	13.4	14.2	14.6 ± 0.6	−121	0.3	3
Hull	F-G	16.9	11.8 ± 0.7	10.1[5]	9.9	10.5	11.1 ± 0.4	55	−0.2	4
Nickerson	F-G	10.4	7.1 ± 0.4	7.3[5]	7.9	8.6	8.0 ± 0.7	−32	0.1	1
Sulzberger	E′-F	39.4	17.5 ± 1.0	16.7[3]	16.6	16.4	16.6 ± 1.7	37	−0.1	6
Withrow	E′-F	2.4	1.0 ± 0.1	1.3[1]	1.3	1.3	1.3 ± 0.1	−11	0.0	0
Richter	E′-F	0.7	0.5 ± 0.0	0.8[1]	0.8	0.8	0.8 ± 0.1	−11	0.0	0
Ross West	E′-F	788.4	107.2 ± 5.6	96.2[1]	85.2	76.6	72.6 ± 4.2	916	−2.5	194
West Antarctica		2,115	653 ± 38	676	696	741	789 ± 42	−2640	7.3	528
Ross East	E-E′	1,649.5	63.8 ± 3.8	65.2[4]	65.2	64.1	64.1 ± 5.5	−32	0.1	976
David	D′-E	213.5	7.5 ± 0.4	9.5[3]	10.2	9.7	9.2 ±0.4	−84	0.2	118
Lillie	D′-E	15.7	3.2 ± 0.2	3.3[1]	3.4	3.5	3.6 ± 0.2	−11	0.0	2
Rennick	D′-E	52.3	6.1 ± 0.4	6.0[3]	6.0	5.6	5.7 ± 0.5	8	0.0	11
Slava	D′-E	5.0	2.7 ± 0.2	2.9[1]	2.9	2.9	2.9 ± 0.3	−9	0.0	1
Matusevitch	D′-E	17.3	3.9 ± 0.2	4.1[5]	4.2	4.3	4.5 ± 0.2	−16	0.0	6
Cook	D-D′	308.1	37.7 ± 2.2	37.0[3]	40.2	40.7	40.6 ± 2.0	−66	0.2	158
Ninnis	D-D′	178.7	22.4 ± 1.3	23.9[1]	23.1	23.2	23.0 ± 1.0	−34	0.1	95
Mertz	D-D′	84.6	19.3 ± 1.1	18.8[3]	18.2	18.4	17.6 ± 0.8	38	−0.1	37
Dibble	D-D′	32.2	15.6 ± 0.9	18.5[3]	17.7	19.9	19.9±1.4	−129	0.4	12
Frost	C′-D	155.0	43.8 ± 2.6	49.0[4]	46.7	47.3	49.4 ± 1.8	−159	0.4	84
Holmes	C′-D	29.7	16.8 ± 1.0	20.1[1]	19.9	21.9	21.7±1.4	−152	0.4	11
Moscow	C′-D	221.6	46.1 ± 2.7	49.3[3]	50.0	47.5	47.0 ± 2.1	−93	0.3	128
Totten	C′-D	556.0	64.7 ± 3.8	72.6[3]	69.0	69.2	71.4 ± 2.6	−236	0.7	385
Vincennes Bay	C′-D	134.6	34.8 ± 2.1	35.7[4]	36.7	35.6	36.2 ± 0.5	−49	0.1	66
Denman	C-C′	265.5	52.7 ± 3.1	55.4[3]	59.1	57.7	59.2±4.2	−191	0.5	149
West	C-C′	213.7	42.3 ± 2.5	41.9[2]	41.7	41.6	43.1 ± 2.3	6	0.0	115
Publications	C-C′	3.5	5.4 ± 0.3	5.5[1]	5.6	5.8	5.9±0.5	−12	0.0	13
Amery	B-C	1,338.2	75.3 ± 4.4	76.6[5]	77.3	76.7	77.4 ± 3.6	−65	0.2	777
Rayner Thyer	A′-B	118.4	16.6 ± 1.0	17.8[4]	18.6	16.6	16.8 ± 2.1	−32	0.1	54
Shirase	A′-B	207.3	17.9 ± 1.1	18.0[3]	16.7	16.1	16.0 ± 0.7	46	−0.1	118
Baudouin	A-A′	299.6	26.5 ± 1.6	27.2[4]	28.4	26.9	27.1 ± 2.0	−36	0.1	134
Borchgrevink	A-A′	172.3	20.5 ± 1.2	21.3[2]	22.4	20.3	19.9 ± 1.7	−21	0.1	72
Lazarev	A-A′	32.6	6.4 ± 0.4	6.0[4]	5.2	4.9	4.8±0.4	45	−0.1	7
Nivl	A-A′	27.7	4.3 ± 0.3	4.5[3]	4.5	4.2	4.5 ± 0.6	−6	0.0	8
Vigrid	A-A′	35.7	3.7 ± 0.2	3.8[3]	3.7	3.8	3.7± 0.3	−3	0.0	15
Jutulstraumen	A-A′	190.9	29.9 ± 1.8	26.7[3]	29.5	30.6	30.0 ± 2.2	33	−0.1	73
Jelbart	A-A′	20.0	8.2 ± 0.5	9.0[1]	9.8	9.1	9.1 ± 0.8	−41	0.1	3
Atka	K-A	1.4	0.6 ± 0.0	0.9[2]	0.9	0.9	0.9 ± 0.2	−9	0.0	0
Ekstrom	K-A	16.0	4.9 ± 0.3	4.8[3]	4.5	4.5	4.5 ± 0.7	11	0.0	2
Quar	K-A	2.8	0.9 ± 0.1	1.0[1]	1.0	1.0	1.0 ± 0.2	−3	0.0	0
Riiser Larsen	K-A	92.8	18.8 ± 1.1	19.2[4]	19.2	17.0	16.7 ± 2.3	25	−0.1	19
Stancomb Wills	K-A	124.0	22.0 ± 1.3	22.4[2]	21.3	21.5	20.5 ± 1.6	17	0.0	46
Filchner	J″-K	2,146.9	110.1 ± 6.5	110.7[1]	111.3	107.1	106.3 ± 5.7	43	−0.1	1223
East Antarctica		9,794	1,075 ± 63	1,108	1,114	1,100	1,104 ± 69	−1211	3.4	5169
Islands		163.0	77.0 ± 4.5	77.0	77.0	77.0	77.0 ± 4.5	0	0.0	0
Total		12,353	2,098 ± 133	2,163	2,194	2,244	2,306 ± 142	−4,760	13.2	5,725

Area of drainage basin in 10^3 km^2, average SMB for 1979–2008 with 1-σ uncertainty in billions of tons per year, average ice discharge (D) for 1979–1990, 1989–2000, 1999–2010, and 2009–2017 with 1-σ uncertainty in billions of tons per year , cumulative mass gain (M) in billions of tons for 1979–2017, SLR (millimeters) for 1979–2017, and SLR equivalent for each basin (centimeters). Source of ice thickness: [1] Bedmap-2, [2] Mass Conservation, [3] Griggs and Bamber DEM, [4] Balance flux and speed, and [5] Ice floatation from TDX DEM. See complete *SI Appendix*, Table S1 for reference.

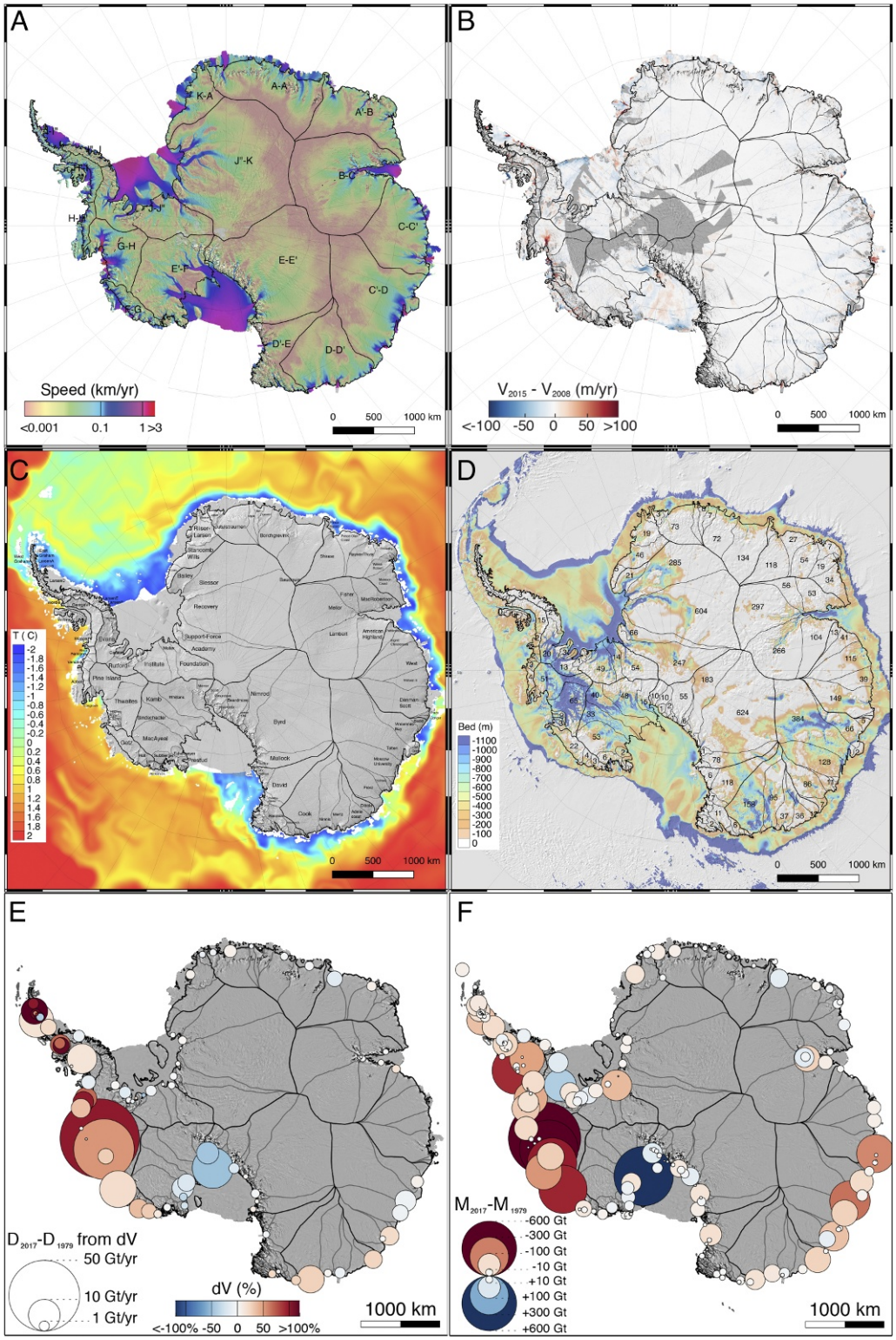

Fig. 1. (*A*) Ice speed of the Antarctic Ice Sheet derived from multisensor data for the time period 2014–2016 (11) with 18 subregions A–K (black thin lines) delineated from surface slope and ice flow direction data (*SI Appendix*, Fig. S3). (*B*) Change in flow speed from the time period 2007–2008 to 2014–2015 color-coded from blue (deceleration) to red (acceleration). Grey areas have no data. (*C*) Basin names for subregions and ocean temperature at 310-m depth from the Southern Ocean State Estimate (SOSE) (12) color-coded from cold (blue) to warm (red). White areas in the ocean are shallower than 310 m depth. (*D*) Bed topography between 0 and 1,100 m depth, with SLE of each basin in centimeters of SLE (1, 13). (*E*) Change in grounding line ice discharge, D, for 1979–2017 for the 18 major subregions in billions of tons per year with percentage change in speed color-coded from red (acceleration) to blue (deceleration) and circle radius proportional to change. (*F*) Total change in mass of major basins color-coded from blue (gain) to red (loss) for 1979–2017 with circle radius proportional to the absolute mass balance.

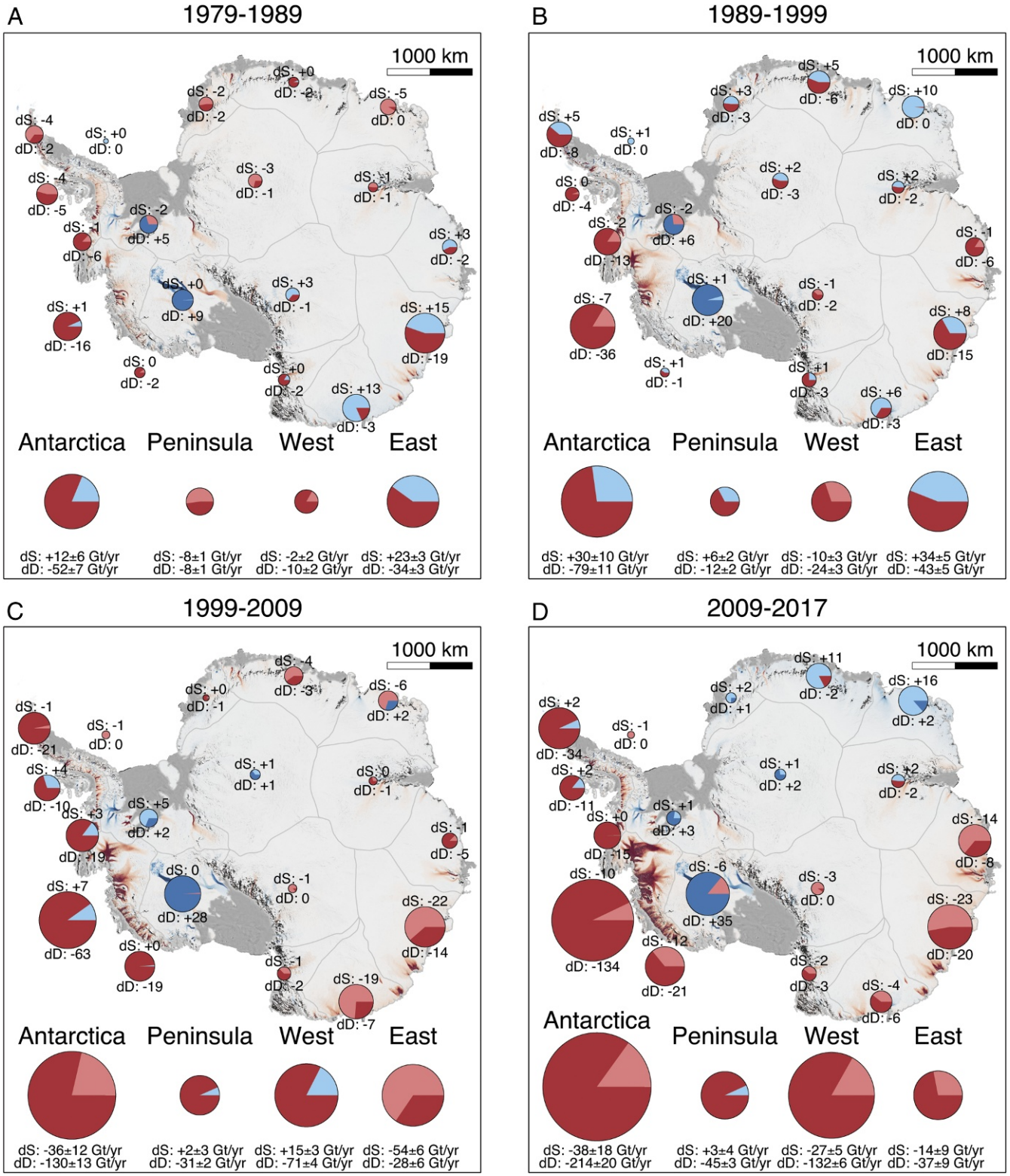

Fig. 2. Ice mass balance of Antarctica using the component method (SMB, on grounded ice minus ice discharge, D, at the grounding line) for (*A*) 1979–1990, (*B*) 1989–2000, (*C*) 1999–2009, and (*D*) 2009–2017. The size of the circle is proportional to the absolute magnitude of the anomaly in D (dD = $SMB_{1979-2008}$ − D) or SMB (dSMB = SMB − $SMB_{1979-2008}$). The color of the circle indicates loss in dD (dark red) or dSMB (light red) versus gain in dD (dark blue) or dSMB (light blue) in billions of tons (10^{12} kg) per year. Dark color refers to dD; light color refers to dSMB. Plots show totals for Antarctica, Antarctic Peninsula, West Antarctica, and East Antarctica. Background is the total mass balance spread into the drainage basins color-coded from red (loss) to blue (gain).

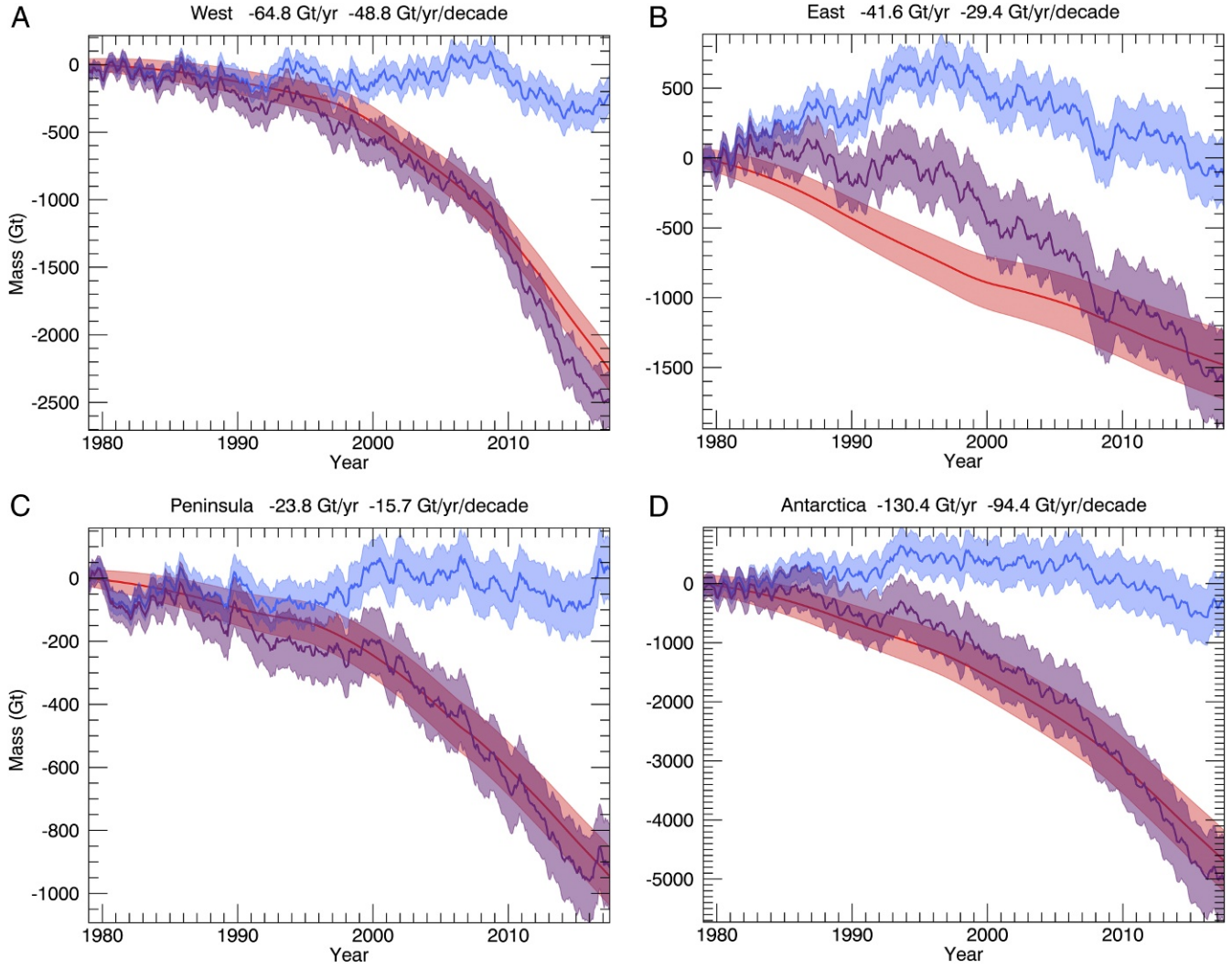

Fig. 3. Time series of cumulative anomalies in SMB (blue), ice discharge (D, red), and total mass (M, purple) with error bars in billions of tons for (*A*) West Antarctica, (*B*) East Antarctica; (*C*) Antarctic Peninsula), and (*D*) Antarctica, with mean mass loss in billions of tons per year and an acceleration in billions of tons per year per decade for the time period 1979 to 2017. The balance discharge is $SMB_{1979-2008}$. Note that the total mass change, M = SMB − D, does not depend on $SMB_{1979-2008}$.

48 Gt/y per decade in 1979–2001 to 134 Gt/y per decade in 2001–2017, or 280%. Most of the 1979–2017 acceleration is from West Antarctica (48 Gt/y per decade), followed by East Antarctica (29 Gt/y per decade) and the Antarctic Peninsula (16 Gt/y per decade) (Fig. 3). In 2009–2017, West Antarctica contributed 63% of the total loss (159 ± 8 Gt/y), East Antarctica 20% (51 ± 13 Gt/y), and the Peninsula 17% (42 ± 5 Gt/y) (Table 2). The mass loss from West Antarctica is three to four times larger than that from East Antarctica and the Peninsula, respectively. We find that the Antarctic Ice Sheet has been out of balance with snowfall accumulation the entire period of study, including in East Antarctica.

In partitioning the mass budget, the SMB dominates the interannual to decadal variability in mass balance. Following a period of relatively positive SMB anomalies in the 1970s–1990s, Antarctica experienced negative SMB anomalies in the 1990s–2017 (Fig. 2 and Table 2). Decadal variability in SMB has been pronounced in East Antarctica. For instance, in Queen Maud Land, a large snowfall event in 2009 added 200 Gt of mass to the ice sheet (14) (*SI Appendix*, Fig. S4). Ice dynamics, however, drove the mass loss on decadal time scales in West Antarctica (89%), East Antarctica (97%), and the Peninsula (94%).

In the remainder of the paper, basin by basin, we discuss anomalies in ice discharge or dynamic losses, dD, which is the average SMB from the reference years 1979–2008, $SMB_{1979-2008}$, minus ice discharge, D. A negative anomaly in ice discharge means that the glacier discharge is above that which would maintain it in mass equilibrium with the average accumulation of snowfall in the interior over the time period 1979–2008. We similarly discuss anomalies in SMB, dSMB, which is SMB − $SMB_{1979-2008}$, to characterize the variations in SMB in reference to a balance accumulation $SMB_{1979-2008}$. The total mass balance, SMB − D, does not depend on the reference $SMB_{1979-2008}$. $SMB_{1979-2008}$ is only used to estimate anomalies in D and SMB. All mass losses refer to land ice (i.e., exclude the mass loss on ice shelves) (3), even though many basins are named after an ice shelf.

Antarctic Peninsula. In Basin I-I″, glaciers in West Graham Land increased their ice discharge by 12% in 1993–2003 (15) and 8% in 2003–2016. We cannot quantify the loss in 1973–1993, but the glaciers were retreating at that time (16). In East Graham Land, there is too much uncertainty in thickness, speed, and SMB to estimate mass balance, but the balance discharge is only 3.3 Gt/y

Table 2. Mass balance (dM = SMB − D) and anomaly in ice discharge dD = $SMB_{1979-2008}$ − D for West Antarctica, Antarctica Peninsula, East Antarctica, and Antarctica over decadal time scales from 1979–2017 in billions of tons per year and total contribution to SLR in millimeters (1 mm = 360 Gt/y)

dM, dD	1979–1989, Gt/y	1989–1999, Gt/y	1999–2009, Gt/y	2009–2017, Gt/y	1979–2017, mm
West Antarctica	−11.9 ± 3	−34.0 ± 4	−55.6 ± 5	−158.7 ± 8	6.9 ± 0.6
	−9.9 ± 2	−23.7 ± 3	−70.6 ± 4	−131.9 ± 6	
Peninsula	−16.0 ± 2	−6.2 ± 3	−29.1 ± 3	−41.8 ± 5	2.5 ± 0.4
	−7.6 ± 1	−12.1 ± 2	−31.3 ± 2	−45.1 ± 3	
East Antarctica	−11.4 ± 4	−9.2 ± 7	−81.8 ± 9	−51.0 ± 13	4.4 ± 0.9
	−34.5 ± 3	−43.3 ± 5	−28.2 ± 6	−36.7 ± 9	
Antarctica	−40.0 ± 9	−49.6 ± 14	−165.8 ± 18	−251.9 ± 27	13.9 ± 2.0
	−52.0 ± 7	−79.3 ± 11	−130.2 ± 13	−213.9 ± 20	

so the mass loss is likely smaller than that. Farther south, the northern Larsen A glaciers lost 1 Gt/y after the ice-shelf collapse in 1995, but only over a short period (17). In contrast, the 4-Gt/y mass loss of Drygalski Glacier has continued from 1995 to present. The Larsen B glaciers accelerated in 2002 when the ice shelf collapsed and were still losing 8.4 Gt/y in 2017 (18, 19). We estimate a small dynamic loss for the Larsen C glaciers (1 Gt/y) and negligible loss for the Larsen D–G glaciers (basin I″-J) (Dataset S1 and Fig. 1). These areas do not hold much SLE (Table 1).

In the west, the glaciers feeding Wordie Ice Shelf (1.3-cm SLE) lost 1 to 2 Gt/y in 1979–2003, increasing to 8 Gt/y in 2017, with speed-up detected over the entire drainage. The mass loss for Wilkins Ice Shelf is small since the glaciers melt completely at their grounding line and do not speed up (20).

For the much larger George VI and Stange ice shelves (basin H′-I), with a combined SLE of 17 cm, we estimate significant glacier losses of 9 and 2 Gt/y in 2017, respectively, versus balance fluxes of 70 ± 4 and 16 ± 1 Gt/y. Riley, Millet, Ryder, Goodenough, and AN77204S6636W sped up in the north in the mid-2000s. Three large glaciers (AN77252S6729W, AN77319S7007W, and AN77326S6324W) with deep basins sped up in the south (21, 22), while Nikitin and Hall glaciers sped up into Stange Ice Shelf.

Overall, the cumulative mass loss from the Antarctic Peninsula is dominated by the West coast (George VI, West Graham Land, Wordie, and Stange) and Larsen A and B since 1995 and 2002, for a total 2.5 ± 0.4-mm SLR since 1979. The mass loss tripled after the 1990s, averaged 24 Gt/y in 1979–2017, with an acceleration of 16 Gt/y per decade.

West Antarctica. Inthe Bellingshausen Sea (BS) (basin H-H′), significant glacier changes on Fox (1-cm SLE) and Ferrigno (2-cm SLE) glaciers since 1979 have doubled their mass loss to 11 Gt/y in 2017. The glaciers flowing into Venable Ice Shelf (3-cm SLE) slowed down in recent years, lowering their loss from 4 to 3 Gt/y. Abbot Ice Shelf doubled its mass loss from 2 to 4 Gt/y with glacier speed-up, consistent with reports of retreating grounding line (23). Farther west (basin G-H), the dominant mass loss is from the Amundsen Sea Embayment (ASE), as reported extensively elsewhere (24, 25). Pine Island, Thwaites, Haynes, Pope, Smith, and Kohler hold a combined 125-cm SLE and experienced a 136 Gt/y loss in 2017, with a disproportionate contribution from Dotson and Crosson ice shelves (94% and 228% of the balance flux versus 78% for Pine Island, 44% for Thwaites, and 49% for Haynes). The loss from Pine Island has stabilized since 2012 but remains the largest loss (58 Gt/y) in Antarctica and elsewhere (37 Gt/y for Thwaites and 32 Gt/y for Kohler/Smith).

A new result is the mass loss from Getz Ice Shelf (22-cm SLE, basin F-G) of 16.5 Gt/y in 2017, or 23% of its balance flux versus 5 Gt/y in 1979–2003 (i.e., a tripling in mass loss). We detect a progressive acceleration of Brennen Inlet, three unnamed glaciers (ANT77452S12220, ANT77453S124427W, and ANT77446S12656W), and especially DeVicq, Berry, and Venzke on the western flank (Fig. 1). Farther west, glacier speed-up and enhanced losses are detected on Hull (18% out of balance) and Land (14%), but the glaciers draining into Nickerson (1-cm SLE) and Sulzberger (6-cm SLE) ice shelves yield no evidence for mass loss or speed-up.

On the west Ross Ice Shelf (basin E′F), we have a unique situation along Siple Coast (194-cm SLE), where the glaciers have continued their slow down starting from a state of balance in the 1970s, with a mass gain reaching 20 Gt/y mass gain in 2017. In the drainage of Ronne Ice Shelf (basin J-J″, 158-cm SLE), we find no change in glacier speed and a negligible mass gain over the entire period (26).

In total, the mass loss of West Antarctica is dominated by a sector spanning from George VI to Land glaciers, about 2,400 km in length, with 92% of the signal from the ASE. West Antarctica contributed 6.9 ± 0.6-mm SLR since 1979.

East Antarctica. On East Ross Ice Shelf (basin E-E′, 976-cm SLE), we detect no change in speed since the 1960s, as in ref. 27. We confirm a speed-up of Byrd in 2009 during a lake drainage event (28). In Victoria Land (basin D′E), David Glacier (118-cm SLE) fluctuated at the 10% level with a small mass loss. With the RACMO2.1 SMB model, the balance flux of David Glacier was 57% too high. The improved modeling of wind transport of snow in RACMO2.32p1 confirms a lower-than-average snowfall accumulation (29) and a balance flux closer to the glacier discharge. We have no evidence for mass loss in Victoria Land based on velocity changes or ice front position (30), except for Matusevitch Glacier, which sped up in 2008, losing 1 Gt/y in 2017, or 27% of its balance flux.

In basin D-D′, the glaciers draining into Cook Ice Shelf (158-cm SLE) averaged a 2 to 3 Gt/y dynamic loss over the survey period. The western Cook Ice Shelf disintegrated in the 1970s (31). Glacier flow was high in the 1980s, decreased in the 1990s, and increased in the 2000s. Farthest west, the glaciers draining into Ninnis (95-cm SLE) and Mertz (37-cm SLE) followed opposite trends: a small loss for Ninnis versus a small gain for Mertz. Ninnis ice tongue broke up in 2008, followed by speed-up, whereas Mertz lost a part of its floating tongue in 2013 but did not speed up. We detect no significant signal along Adelie Coast (36-cm SLE), which hosts few ice shelves.

In basin C′-D, Dibble (12-cm SLE), Frost (84-cm SLE), and De Haven and Holmes (11-cm SLE) combine for a dynamic loss of 12.7 Gt/y in 2017 versus 9 Gt/y in 1979–2003. Frost and Holmes develop small ice shelves that regularly disintegrate in warmer-than-usual summers (32). The glacier draining into Moscow University Ice Shelf (128-cm SLE) shows little change, with a 3 Gt/y loss in 1979–2003 versus a 0.3 Gt/y gain in 2017. This situation contrasts with Totten Glacier (385-cm SLE), which slowed down from the 1990s to 2000s, sped up until 2009,

and slowed down again until recently, while maintaining speeds above those in year 2000. Totten mass loss has increased through time but remains at about 10% of the balance flux (33), increasing from 5.7 Gt/y in 1979–2003 to 7.3 Gt/y in 2003–2017. In Vincennes Bay (66-cm SLE), Vanderfjord, Adams, Anza, Bond, and Underwood develop fast flow near the coast, with short floating sections that vary in extent through time (32). Bond and Underwood have changed the most, accelerating in 2008–2016, from a lowest ice discharge in 1996. Vanderfjord experienced a spectacular grounding line retreat of 17 km between 1996 an 2017 (*SI Appendix*, Fig. S2).

Significant changes have taken place on Denman Glacier and Shackleton Ice Shelf, which hold a 149-cm SLE (basin C-C′). Denman sped up 16% since the 1970s and the ice shelf sped up by 33% in 1957–1996 and 43% in 1957–2016. The glacier is 10% out of balance. Its neighbor Scott decelerated by 16% in 1957–1996 and 22% in 2000–2008 and sped up by 18% in 2016. Farther west, West Ice Shelf (115-cm SLE) is near balance, but its largest glacier, Philippi, is flowing above equilibrium and losing mass. Publication Ice Shelf (13-cm SLE) has only a slightly negative mass balance. Amery Ice Shelf (basin B-C) (777-cm SLE) is in balance, with velocities remarkably similar to those measured in the 1970s. Enderby Land (basin A′-B) has few ice shelves. We detect speed-up on Wilma-Robert (19-cm SLE) and Rayner (54-cm SLE) in 2008–2016, with Rayner losing 0.7 Gt/y or 7% of its mass flux. Shirase Glacier (118-cm SLE) is near balance despite fluctuations in speed at the 20% level with changes in its floating ice tongue. We have no evidence for long-term change in Queen Maud Land (basin A-A′) and only a small mass loss for Jutulstraumen (73-cm SLE) and neighbors to the west (6-cm SLE) and Riiser-Larsen Ice Shelf (basin K-A) (19-cm SLE) (Table 1 and Dataset S1). Stancomb-Wills Glacier (basin K-A) varies in speed at the 5 to 19% level due to time-dependent interactions with the slow-moving Brunt Ice Shelf and the ice melange in between (34), but the resulting loss is negligible. Finally, the basin of Filchner Ice Shelf (basin J′′-K, 1,223-cm SLE) is in balance, with glacier velocities fluctuating at the 2 to 3% level (*SI Appendix*, Fig. S4). In total, the mass loss in East Antarctica is dominated by Wilkes Land, with a total contribution of 4.4 ± 0.9-mm SLR since 1979.

Discussion

The mass loss of Antarctica is dominated by the ASE and BS sectors, in West Antarctica, Wilkes Land, in East Antarctica, and the western Peninsula and Larsen A and B sectors (Figs. 2 and 3 and *SI Appendix*, Fig. S4). In the ASE and BS, the glacier changes are widespread and synchronous. They have been attributed to the intrusion of warm, salty, circumpolar deep water (CDW) on the continental shelf (35, 36), which vigorously melts the ice shelves, reduces buttressing of the glaciers, and allows them to flow faster. The presence of CDW has been well documented on the Western Peninsula (37, 38), BS (39), ASE (40), and Getz (41), but not on Sulzberger and Ross (40), which indeed exhibit low ice-shelf melt and no mass loss. We posit that Nickerson Ice Shelf marks the western limit of the influence of CDW on West Antarctic ice shelves since it experiences near-zero mass balance and low ice-shelf melt rates. The sea floor in front of Nickerson Ice Shelf is shallower than farther east and must block the access of warm CDW (Fig. 1). Similarly, there is no evidence for the presence of CDW in the Larsen C-G sectors (42) and only small mass losses.

The mass loss in ASE, BS, Wilkes, and Western Peninsula have been increasing since the 1970s. This evolution is consistent with the polar contraction of the westerlies that force more CDW on the continental shelf through Ekman transport, which reaches the glaciers through deep troughs carved on the sea floor by former ice streams (Fig. 1) (43), melts the ice shelves, and destabilizes the glaciers. In the ASE, Pacific decadal oscillations modulate the ocean heat transfer and subsequent glacier loss, which explains the higher loss in 2002–2009 followed by a lower loss in 2010–2016 (44, 45). We find that ASE was near balance in the 1970s, however, which contradicts the hypothesis that an instability developed in the 1940s until the 1970s (46). We conclude that the recent rapid loss is unique over the last several decades.

The high loss of Fox and Ferrigno is consistent with efficient CDW transport through the Belgica trough (47), whereas Abbot Ice Shelf floats on a seafloor above the depth of CDW (>400–700 m), which explains its low ice-shelf melt rates and limited mass loss of the glaciers (48). Similarly, we find the largest loss and acceleration on the western sector of Getz, which is more exposed to incoming CDW than the eastern sector (40). High mass losses in this sector are caused by nearly undiluted CDW, manifest with high ice-shelf melt rates (3). Conversely, areas farthest from CDW (e.g., Ross and Filchner Ice Shelves) are stable and exhibit no loss. A number of areas potentially exposed to CDW do not melt rapidly (e.g., Wilkins and Nickerson), as stated earlier, most likely because the sea floor depth is too shallow to enable the access of warm CDW to grounding lines.

Our mass balance numbers are within errors of the IMBIE-2 multisensor assessment for the years 1992–2017 (10) for West Antarctica (−83.7 ± 8 Gt/y versus −94 ± 27 Gt/y) and the Peninsula (−28.3 ± 1 Gt/y versus −20 ± 15 Gt/y), but our overall losses are higher for Antarctica (168.9 ± 5 Gt/y for 1992–2017 versus 109 ± 56 Gt/y) because we report a loss for East Antarctica (−57.0 ± 2 Gt/y) versus a gain with a large uncertainty in the IMBIE-2 assessment (+5 ± 46 Gt/y) (Table 1). Our estimate is affected by uncertainties in ice thickness and SMB but the errors are low when estimating decadal trends. Improved SMB models and additional ice thickness data in East Antarctica would further reduce uncertainties. The IMBIE-2 altimetry estimate, however, is affected by large uncertainties in translating volume changes into mass changes, especially in East Antarctica. With accumulation levels at the 5 cm/y level on the high plateau (basin B-C), decades of altimetry data will be required to detect changes in SMB at the 10% level (5 mm/y or 5 cm per decade). Similarly, the IMBIE-2 gravity estimate is affected by residual uncertainties in correction for the glacial isostatic adjustment (GIA), especially in East Antarctica. Revisions of the GIA correction of the order 10–50 Gt/y would suffice to reconcile the Gravity Recovery and Climate Experiment results with our mass balance numbers.

An emerging result is the dynamic loss from Wilkes Land, East Antarctica. We detect a mass loss not only in the last few years (49, 50) but over the entire period, with even higher losses in the 1980s. This evolution is corroborated with the degradation of major ice shelves during that time period: Cook lost half of its ice shelf in the 1970s (31), Frost/Holmes disintegrate regularly in low-sea-ice years (32), and Conger/Glenzer, Shackleton, and West ice shelves have experienced large retreats between 1962 and the early 1980s (51) that were not compensated by a readvance in subsequent decades.

We have incomplete information about the presence CDW in this sector of East Antarctica (52). A recent survey found modified CDW in front of Totten (53). Totten is protected from a fast retreat into a deep marine basin by a prograde slope for the first 50 km (33) and hence is at low risk of developing a marine instability in the near future. In contrast, Denman is grounded on a ridge with a steep retrograde slope immediately upstream. There are no oceanographic data near the glacier, but the ice shelf experiences high melt rates, which suggests the presence of modified CDW. The recent ice-shelf speed-up may reveal enhanced intrusion of CDW and an increase in ice-shelf melt or may result from complex interactions between the fast-moving portion of Shackleton Ice Shelf and the surrounding slower-moving ice shelf, as for the Stancomb-Wills Glacier (34).

To the East of Denman, the troughs occupied by Ninnis and Cook hold the most potential for rapid retreat if CDW can access the glaciers (Fig. 1*D*). To the west of Denman, West Ice Shelf appears to be stable or changing slowly, suggesting that CDW does not have easy access to the cavity, but the bathymetry beneath and in front of the ice shelf is unknown (Fig. 1*D*).

Table 1 lists the major glacier systems in terms of mass balance, cumulative mass loss, and SLE (more details are given in Dataset S1). Sectors with significant SLE include ASE (125 cm), Getz (22 cm), George VI (15 cm), Land/Hull (7 cm), and Fox/Ferrigno (5 cm) in West Antarctica and the Peninsula, but only the ASE may be conducive to marine ice sheet instability (i.e., includes bed channels extending well below sea level in the deep interior along mostly retrograde slopes). The northern Peninsula does not hold a large SLE: 4 mm for Larsen B, 1 cm for Larsen C, and 5 cm for Larsen D-G. Sectors with weak potential include Totten (385 cm) and Vanderfjord Glacier in Vincennes Bay (66 cm) because they are protected by prograde bed slopes (33). Sectors at risk and requiring more observation include West Ice Shelf (115-cm SLE), Denman/Shackleton Ice Shelf (149-cm SLE), Cook (158-cm SLE), and Ninnis (95-cm SLE). In sum, the northern sector of West Antarctica is losing mass rapidly and could entrain the progressive collapse of a large share of West Antarctica and its 5.1-m SLE. In Wilkes Land, East Antarctica, the ice sheet loss is two to three times slower, but this sector holds an equally large, multimeter SLE.

Over the last four decades, the cumulative contribution to sea level from East Antarctica is not far behind that of West Antarctica, that is, East Antarctica is a major participant in the mass loss from Antarctica despite the recent, rapid mass loss from West Antarctica (Table 1). Our observations challenge the traditional view that the East Antarctic Ice Sheet is stable and immune to change. An immediate consequence is that closer attention should be paid to East Antarctica.

In the decades to come, it is likely that SLR from Antarctica will originate from the same general areas, which are nearest to the sources of warm CDW and therefore directly sensitive to a strengthening and contraction of the polar westerlies toward Antarctica that bring more CDW in contact with the glaciers. As ice-shelf melt increases, the glaciers will feel less resistance to flow, accelerate, and contribute to SLR.

Conclusions

Using revised inventories, improved thickness mapping, and time series of velocity and SMB, we present four decades of mass balance in Antarctica that reveal a mass loss during the entire period and a rapid increase over the last two decades in parts of Antarctica closest to known or suspected sources of CDW from observations of high ice-shelf melt rates, ocean temperature, or based on ocean model output products. This evolution of the glaciers and surrounding ice shelves is consistent with a strengthening of the westerlies caused by a rise in greenhouse gas levels and ozone depletion that bring more CDW on the continental shelf. While the mass loss from the Peninsula and West Antarctica have been well documented and reported elsewhere, we note that the Wilkes Land sector of East Antarctica has been a major participant to SLR over the last 40 y, with larger losses in the 1980s. These sectors are all close to CDW and experiencing high ice-shelf melt rates. Enhanced intrusion of CDW being the root cause of the mass loss in the ASE and the West Peninsula, we posit that a similar situation is taking place in Wilkes Land, where novel and sustained oceanographic data are critically needed. Our mass balance assessment, combined with prior surveys, suggests that the sector between Cook/Ninnis and West ice shelves may be exposed to CDW and could contribute multimeter SLR with unabated climate warming.

Materials and Methods

Ice Velocity, Thickness, and Discharge. The first comprehensive velocity map of Antarctica combined data from multiple satellite sensors at different epochs (54). We use a time series of yearly averaged ice-sheet velocity that spans from 1992 to 2017 with an error of a few meters per year calculated from a weighted average by instrument (11). For 1979–1989, we use Landsat MSS 1–5 and TM 4–5 data (SI) with errors in speed of 10–20 m/y. Ice thickness is from (*i*) BEDMAP-2 (1); (*ii*) BedMachine Antarctica (13), which combines radar-derived thickness with ice motion vectors, SMB, and ice elevation changes from altimetry; and (*iii*) ice-shelf thickness based on ERS-1 altimetry data from the year 1994 (55) or from (*iv*) a TanDEM-X (TDX) DEM of Antarctica from May–July 2013 and 2014 at 30-m spacing (56). If ice thickness is not of sufficient quality, we assume a 1979 ice flux in balance with the average SMB for 1979–2008 and scale the results based on changes in ice velocity. We constrain fluxes with ice thickness and time-variable velocity for 78% of Antarctic Peninsula, 96% of West Antarctica, and 79% of East Antarctica. We use a 10-m uncertainty in thickness for direct radar measurements and 30 m for hydrostatic equilibrium as in ref. 7. We use a reference velocity map from ref. 3 to calculate reference fluxes. We compare the reference velocity with velocity data from different years to calculate a scaling factor over the fastest parts of the glacier and apply the results to the reference flux to obtain time series of yearly ice fluxes.

Ice Drainage, SMB, and Total Mass Balance. We use a TDX DEM smoothed over 10 ice thicknesses to derive drainage boundaries based on surface slope (56). In places where flow direction is known with confidence (errors less than 2°) we replace the direction of surface slope with the flow direction from a reference velocity of Antarctica (*SI Appendix*, Fig. S3). We use the RACMO2.3p1 in our assessment. Total mass balance, SMB − D, of grounded ice in each basin is summed up by regions (A–K), East, West, Peninsula, and for all of Antarctica. We calculate a mean mass loss on a decadal time scale by fitting the time series of monthly data and measurement errors with a linear regression. The slope of the regression is the mean mass loss for the decade and the 1-σ value of the regression is the error of the calculated decadal mass loss. Over the entire period 1979–2017, we perform a quadratic regression to obtain a mean mass loss and an acceleration in mass loss per decade. Cumulative dSMB and dD values are calculated in reference to SMB for the 1979–2008 reference period. The velocity, grounding line data, and drainage basins are available at National Snow and Ice Data Center (NSIDC), Boulder, CO as MEaSURES-2 products. The ice-thickness data are publicly available from NSIDC, BEDMAP-2, and other references.

ACKNOWLEDGMENTS. We thank the Polar Space Task Group, European Space Agency, Canadian Space Agency, and Japan Aerospace Exploration Agency from the Synthetic Aperture Radar data and German Aerospace Center/Airbus for the TDX DEM used in this study. This work was performed at the University of California Irvine and at California Institute of Technology's Jet Propulsion Laboratory under a contract with the National Aeronautics and Space Administration Cryosphere Science (NNX13AI84A) and MEaSUREs (NNX13AI84A) program. M.v.d.B. acknowledges funding from the Polar Program of The Netherlands Organization for Scientific Research and The Netherlands Earth System Science Centre.

1. Fretwell P, et al. (2013) Bedmap2: Improved ice bed, surface and thickness datasets for Antarctica. *Cryosphere* 7 375–393.
2. Wessem JMv, et al. (2018) Modelling the climate and surface mass balance of polar ice sheets using RACMO2, part 2: Antarctica (1979-2016). *Cryosphere* 12:1479–1498.
3. Rignot E, Jacobs S, Mouginot J, Scheuchl B (2013) Ice-shelf melting around Antarctica. *Science* 341:266–270.
4. Liu Y, et al. (2015) Ocean-driven thinning enhances iceberg calving and retreat of Antarctic ice shelves. *Proc Natl Acad Sci USA* 112:3263–3268.
5. Van de Berg WJ, van den Broeke MR, Reijmer CH, van Meijgaard E (2006) Reassessment of the Antarctic surface mass balance using calibrated output of a regional atmospheric climate model. *J Geophys Res* 111:D11104.
6. Velicogna I, Sutterley TC, van den Broeke MR (2014) Regional acceleration in ice mass loss from Greenland and Antarctica using GRACE time-variable gravity data. *Geophys Res Lett* 4:8130–8137.
7. Rignot E, et al. (2008) Recent Antarctic ice mass loss from radar interferometry and regional climate modelling. *Nat Geosci* 1:106–110.

8. Rignot EJ, Velicogna I, van den Broeke MR, Monaghan AJ, Lenaerts JTM (2011) Acceleration of the contribution of the Greenland and Antarctic ice sheets to sea level rise, *Geophys Res Lett* 38 L05503.
9. Shepherd A, et al. (2012) A reconciled estimate of ice-sheet mass balance. *Science* 338:1183–1189.
10. Shepherd A, et al. (2018) Mass balance of the Antarctic ice sheet from 1992 to 2017. *Nature* 558:219–221.
11. Mouginot J, Rignot E, Scheuchl B, Millan R (2017) Comprehensive annual ice sheet velocity mapping using Landsat-8, Sentinel-1, and RADARSAT-2 data. *Remote Sens* 9:364–1370.
12. Mazloff MR, Heimbach P, Wunsch C (2010) An eddy-permitting southern ocean state estimate. *J Phys Ocean* 40:880–899.
13. Millan R, Rignot E, Bernier V, Morlighem M (2017) Bathymetry of the Amundsen Sea Embayment sector of West Antarctica from operation IceBridge gravity and other data. *Geophys Res Lett* 44:1360–1368.
14. Medley B, et al. (2017) Temperature and snowfall in western Queen Maud Land increasing faster than climate model projections. *Geophys Res Lett* 45:1472–1480.
15. Pritchard HD, Vaughan DG (2007) Widespread acceleration of tidewater glaciers on the Antarctic Peninsula. *J Geophys Res* 112:F03S29.
16. Cook AJ, et al. (2016) Ocean forcing of glacier retreat in the western Antarctic Peninsula. *Science* 353:283–286.
17. Seehaus T, Sebastian M, Helm V, Skvarca P, Brauna M (2015) Changes in ice dynamics, elevation and mass discharge of Dinsmoor-Bombardier-Edgeworth glacier system, Antarctic Peninsula. *Earth Planet Sci* 427:125–135.
18. Rignot E, et al. (2004) Accelerated ice discharge from the Antarctic Peninsula following the collapse of Larsen B ice shelf. *Geophys Res Lett* 31:L18401.
19. Rott H, et al. (2014) Mass changes of outlet glaciers along the Nordensjkold Coast, northern Antarctic Peninsula, based on TanDEM-X satellite measurements. *Geophys Res Lett* 41:8123–8129.
20. Padman L, et al. (2012) Oceanic controls on the mass balance of Wilkins Ice Shelf, Antarctica. *J Geophys Res* 117:C01010.
21. Wouters B, et al. (2015) Dynamic thinning of glaciers on the southern Antarctic Peninsula. *Science* 348:899–903.
22. Hogg A, et al. (2017) Increased ice flow in Western Palmer Land linked to ocean melting *Geophys Res Lett* 44 4159–4167.
23. Christie FDW, Bingham RG, Gourmelen N, Tett SFB, Muto A (2016) Four-decade record of pervasive grounding line retreat along the Bellingshausen margin of West Antarctica *Geophys Res Lett* 43:5741–5749.
24. Mouginot J, Rignot EJ, Scheuchl B (2014) Sustained increase in ice discharge from the Amundsen Sea Embayment, West Antarctica, from 1973 to 2013, *Geophys Res Lett* 201241:1576–1584.
25. Sutterley TC, et al. (2014) Mass loss of the Amundsen Sea Embayment of West Antarctica from four independent techniques. *Geophys Res Lett* 41:8421–8428.
26. Scheuchl B, Mouginot J, Rignot E (2012) Ice velocity changes in the Ross and Ronne sectors observed using satellite radar data from 1997 and 2009. *Cryosphere* 6:1019–1030.
27. Stearns L (2011) Dynamics and mass balance of four large East Antarctic outlet glaciers. *Ann Glaciol* 52:116–125.
28. Stearns LA, Smith BE, Hamilton GS (2008) Increased flow speed on a large East Antarctic outlet glacier caused by subglacial floods. *Nat Geosci* 1:827–831.
29. Stenni B, et al. (2000) Snow accumulation rates in northern Victoria Land, Antarctica, by firn-core analysis. *J Glaciol* 46:541–552.
30. Lovell AM, Stokes CR, Jamieson SSR (2017) Sub-decadal variations in outlet glacier terminus positions in Victoria Land, Oates Land and George V Land, East Antarctica (1972–2013). *Antarctic Sci* 29:468–483.
31. Frezzotti M, Cimbelli A, Ferrigno JG (1998) Ice-front change and iceberg behaviour along Oates and George V Coasts, Antarctica, 1912–96. *Ann Glaciol* 27:643–650.
32. Miles BWJ, Stokes CR, Jamieson SSR (2017) Simultaneous disintegration of outlet glaciers in Porpoise Bay (Wilkes Land), East Antarctica, driven by sea ice break-up. *Cryosphere* 11:427–442.
33. Li X, Rignot E, Mouginot J, Scheuchl B (2016) Ice flow dynamics and mass loss of Totten Glacier, East Antarctica from 1989 to 2015. *Geophys Res Lett* 43:6366–6373.
34. Khazendar A, Rignot E, Larour E (2009) Roles of marine ice, rheology, and fracture in the flow and stability of the Brunt/Stancomb-Wills Ice Shelf. *J Geophys Res* 114:F04007.
35. Jenkins A, et al. (2016) Decadal ocean forcing and antarctic ice sheet response: Lessons from the Amundsen Sea. *Oceanography* 29:106–117.
36. Alley R, et al. (2015) Oceanic forcing of ice-sheet retreat: West Antarctica and more. *Ann Rev Earth Planet Sci* 43:207–231.
37. Moffat C, Owens B, Beardsley RC (2009) On the characteristics of circumpolar deep water intrusions to the west Antarctic Peninsula continental shelf. *J Geophys Res* 114:C05017.
38. Martinson DG, McKee DC (2012) Transport of warm upper circumpolar deep water onto the western Antarctic Peninsula continental shelf. *Ocean Sci* 8:433–442.
39. Zhang X, Thompson AF, Flexas MM, Roquet F, Bornemann H (2016) Circulation and meltwater distribution in the Bellingshausen Sea: From shelf break to coast. *Geophys Res Lett* 43:6402–6409.
40. Jacobs S, et al. (2013) Getz Ice Shelf melting response to changes in ocean forcing. *J Geophys Res* 118:4152–4168.
41. Wahlin AK, Yuan X, Bjork G, Nohr C (2010) Inflow of warm circumpolar deep water in the central Amundsen Shelf. *J Phys Oceanogr* 40:1427–1434.
42. Nicholls KW, Makinson K, Venables EJ (2012) Ocean circulation beneath Larsen C Ice Shelf, Antarctica from in situ observations. *Geophys Res Lett* 39:L19608.
43. Spence P, et al. (2017) Localized rapid warming of West Antarctic subsurface waters by remote winds. *Nat Clim Change* 7:595–603.
44. Greene CA, Blankenship DD, Gwyther DE, Silvano A, van Wijk E (2017) Wind causes Totten Ice Shelf melt and acceleration. *Sci Adv* 3:e1701681.
45. Dutrieux P, et al. (2014) Strong sensitivity of Pine Island ice-shelf melting to climatic variability. *Science* 343:174–178.
46. Smith JA, et al. (2017) Sub-ice-shelf sediments record history of twentieth-century retreat of Pine Island Glacier. *Nature* 541:77–80.
47. Bingham RG, et al. (2012) Inland thinning of West Antarctic Ice Sheet steered along subglacial rifts. *Nature* 487:468–471.
48. Cochran JR, Jacobs SS, Tinto KJ, Bell RE (2014), Bathymetric and oceanic controls on Abbot Ice Shelf thickness and stability. *Cryosphere* 8:877–889.
49. Shen Q, et al. (2018) Recent high-resolution Antarctic ice velocity maps reveal increased mass loss in Wilkes Land, East Antarctica. *Sci Rep* 8:4477.
50. Gardner A, et al. (2017) Increased West Antarctic and unchanged East Antarctic ice discharge over the last 7 years. *Cryosphere* 12:521–547.
51. Young NW, Gibson JAE (2007) A century of change in the Shackleton and West Ice Shelves, East Antarctica. *Geophys Res Abstracts, EGU 2007* 9:10892.
52. Silvano A, Rintoul SR, Herraiz-Borreguero L (2016) Ocean-ice shelf interaction in East Antarctica. *Oceanography* 29:130–143.
53. Rintoul SR, et al. (2016) Ocean heat drives rapid basal melt of Totten Ice Shelf. *Sci Adv* 2:e1601610.
54. Rignot E, Mouginot J, Scheuchl B (2011) Ice flow of the Antarctic Ice Sheet. *Science* 333:1427–1430.
55. Griggs JA, Bamber JL (2011) Antarctic ice-shelf thickness from satellite radar altimetry *J Glaciol* 57:485–497.
56. Rizzoli P, et al. (2017) Generation and performance assessment of the global TanDEM-X digital elevation model. *ISPRS J Photogramm Remote Sens* 132:119–139.